Hindawi Publishing Corporation
International Journal of Antennas and Propagation
Volume 2014, Article ID 471935, 9 pages
http://dx.doi.org/10.1155/2014/471935

Research Article

Fabrication of a 77 GHz Rotman Lens on a High Resistivity Silicon Wafer Using Lift-Off Process

Ali Attaran and Sazzadur Chowdhury

Department of Electrical and Computer Engineering, University of Windsor, CEI 401 Sunset Avenue, Windsor, ON, Canada N9B 3P4

Correspondence should be addressed to Ali Attaran; ali1111@uwindsor.ca

Received 4 December 2013; Accepted 4 April 2014; Published 4 May 2014

Academic Editor: Young Joong Yoon

Fabrication of a high resistivity silicon based microstrip Rotman lens using a lift-off process has been presented. The lens features 3 beam ports, 5 array ports, 16 dummy ports, and beam steering angles of ±10 degrees. The lens was fabricated on a 200 μm thick high resistivity silicon wafer and has a footprint area of 19.7 mm × 15.6 mm. The lens was tested as an integral part of a 77 GHz radar where a tunable X band source along with an 8 times multiplier was used as the RF source and the resulting millimeter wave signal centered at 77 GHz was radiated through a lens-antenna combination. A horn antenna with a downconverter harmonic mixer was used to receive the radiated signal and display the received signal in an Advantest R3271A spectrum analyzer. The superimposed transmit and receive signal in the spectrum analyzer showed the proper radar operation confirming the Rotman lens design.

1. Introduction

Frequency-Modulated Continuous-Wave (FMCW) radar sensors based on analog or digital beamforming technology have been proven to be effective for avoidance of automotive collision or mitigation of collision damage. Investigation shows that instead of using microelectronic based analog or digital beamforming engines, if Rotman lens type passive beamformers can be used, the signal processing time as well as power consumption, size, integration complexity, and system building cost will be reduced significantly [1–5]. Several design approaches are available that propose using Rotman lens for automotive radar applications. However, almost all of them depend on conventional fabrication technique [2] with expensive mass production. Recent investigation shows that high resistivity silicon is an attractive choice to realize high performance millimeter wave MMICs due to lower attenuation and lower cost [4–6]. Additionally, the silicon processing technology is highly matured and the lenses can be batch fabricated like conventional ICs to lower the cost of automotive radars. In [4], a 60 GHz silicon based Rotman lens has been presented. In this context, this paper presents the design procedure of the Rotman lens at mm-frequency range followed by 3D full wave simulation results. Proposed fabricated and tested silicon based Rotman lens is a potential to use in a low cost 77 GHz automotive radar.

2. Rotman Lens Design

Rotman lens is a passive beamforming device and the beam can be steered in a specified direction by selective excitation of any one of the input ports (beam ports) of the lens as shown in Figure 1. Detailed design principles of Rotman lens are well established [4, 7, 8] and can be summarized in 3 major steps.

Step 1. The lens geometrical specifications such as positions of the beam ports on the focal arc and the array ports on the inner contour are determined from the theory of ray optics. Detailed procedure to determine the initial geometry following the ray optics theory is available in [7].

Step 2. Once the initial geometry is determined, the two-dimensional aperture theory of classical antenna analysis is applied to determine electrical characteristics of the lens such as the return loss, insertion loss, port isolation, and power efficiency.

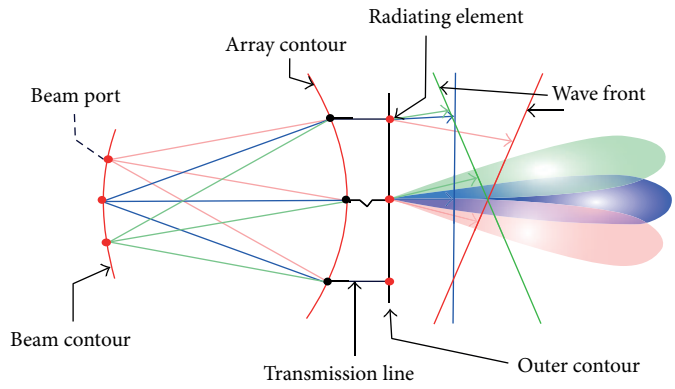

Figure 1: A conceptual diagram of a Rotman lens.

Step 3. Finally, a 3D field solver like HFSS or XFDTD is used to carry out a full-wave analysis that extends the two-dimensional analysis to three-dimensional analysis to incorporate the effects of reflections and scattering from the sidewalls (spillover power) and the lens cavity, surface wave propagation, conductivity of the metal layer, conductive attenuation coefficient, and the dielectric attenuation coefficient [6]. The initial specifications determined in Step 1 are more or less modified at this step to obtain optimum performance.

Following this procedure, for the target automotive application, the lens center frequency has been selected as 77 GHz for use in an automotive radar. For use in a trimode (short-range, mid-range, and long-range) FMCW radar, the lens bandwidth has been selected to be 8 GHz to match the maximum chirp bandwidth of the FMCW signal [5].

Following [9], a scan angle of 10° has been selected to cover an azimuthal angle of 30° at −6 dB of antenna radiation pattern. The number of array port has been chosen to be 5 to minimize the lens width. Following [7], the distance between array elements is calculated to be 0.65λ. This element spacing plays an important role in determining beam width of the microstrip patch antenna arrays. This gives a length of 5.2 mm for $N_{\max}$ which is the farthest output port in the outer contour. Instead of normalizing the parameters with respect to the focal length, following the method presented in [8], the parameters are normalized with respect to the total length of the array aperture:

$$F = 2fN_{\max}\frac{\sin(\beta)}{\sin(\alpha)}, \tag{1}$$

where β is the angular direction of the wave front associated with the perfect focal point at α with respect to the lens axis. To keep the geometry compact, the scan angle β has been chosen to be the same as the focal angle α. Following [8], the ratio of the on-axis and off-axis focal length g has been determined from $g = 1/\cos(\alpha)$ as 1.0154. In [8], it has been shown that, for any value of f as defined in (1), if the focal angle α decreases, the value of g approaches towards unity. For a value of $g = 1.014$ and a scan angle $\alpha = 10°$, f has been determined to be 0.5. In [8], it has also been shown that though the path length error will be at its minimum at $f = 1$ for $15° < \alpha < 60°$, however, for small angles such as 10°–15°, the path length errors can be very small by using a value of f very close to 0.5. By keeping $f \approx 0.5$ a very compact lens can be realized with a little compromise on negligible path length error. To fabricate the lens using microfabrication techniques, the lens geometry needs to be compact to optimize the yield. Consequently, a ratio of 0.53 has been chosen for f that yielded a value for the off-axis focal length F as 5.51 mm. Accordingly, the on-axis focal length G has been determined to be 5.56 mm.

A high resistivity silicon substrate has been chosen to fabricate the lens as it has a very low loss tangent and absorption coefficient [7]. After initial design specifications were set, the lens geometry was simulated in Rotman Lens Designer (RLD) software from Remcom Inc. RLD is a 2D solver that uses the antenna aperture theory to determine electrical losses, lens geometry, microstrip tapers, and transmission line lengths. The design parameters (geometric dimensions and losses) were then optimized by using sidelobe levels, phase errors, and sidewall curvature as the optimizing cost functions. Following (2) below

$$f_t = \frac{150}{\pi h}\sqrt{\frac{2}{\varepsilon_r - 1}}\tan^{-1}\varepsilon_r, \tag{2}$$

where f_t is the cutoff frequency and h is the substrate thickness in millimeters, it was determined that a 200 micrometer thick silicon substrate with a loss tangent of 0.0005 and dielectric constant of 11.8 would yield the optimum results considering port coupling and sidelobe levels. A lower thickness substrate also prevents generation of the spurious surface modes [10].

Considering the microstrip as a quasi-TEM line, the attenuation α_d due to dielectric losses can be determined from [6]

$$\alpha_d = \frac{k_0\varepsilon_r(\varepsilon_e - 1)\tan\delta_d}{2\sqrt{\varepsilon_e}(\varepsilon_r - 1)}\ \text{Np/m}, \tag{3}$$

where $\tan\delta_d$ is the loss tangent. Therefore, a 1.5 micrometer thick gold layer with conductivity 4.52×10^7 S/m was chosen

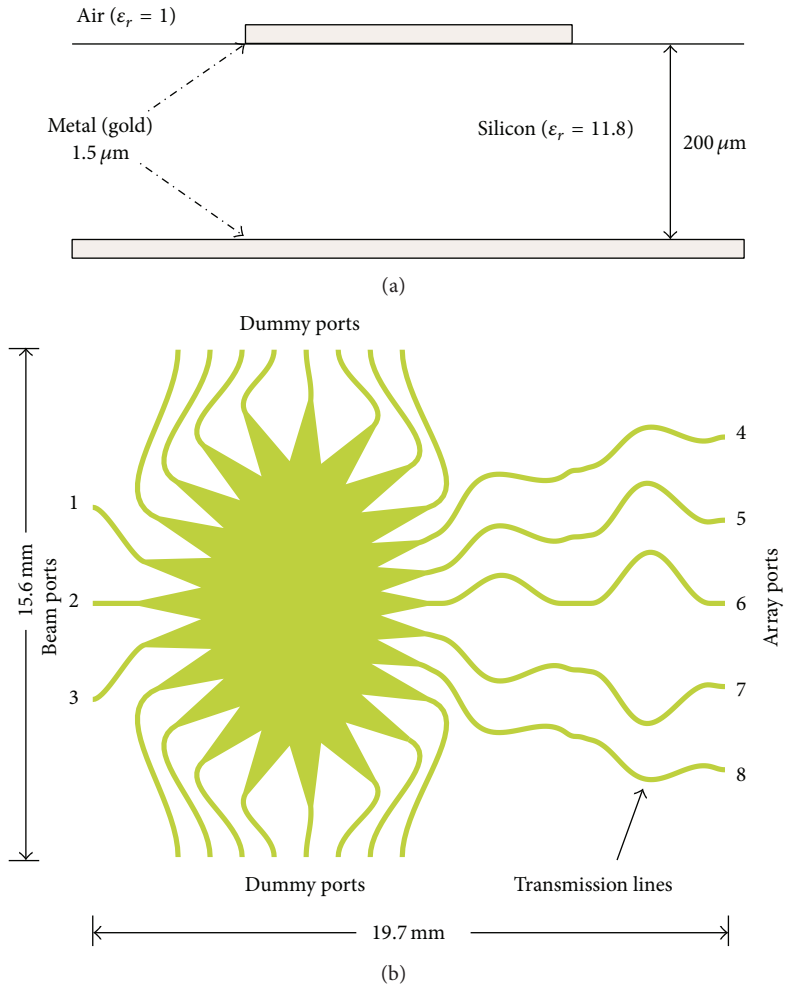

Figure 2: Rotman lens geometry. (a) Cross section. (b) Top view.

Table 1: Rotman Lens Design Specifications.

Parameter	Value
Gold conductor thickness (μm)	1.5
Silicon substrate thickness (μm)	200
Silicon permittivity	11.8
Silicon loss tangent	0.0005
Length (mm) × width (mm)	19.7 × 15.6
Center frequency	77 GHz
Bandwidth	8 GHz
Beamwidth	20°
Focal angle	10°
Scan angle	10°
Beam ports	3
Array ports	5
Dummy ports	16
Element spacing	2.6 mm
Z system	50 ohms
Port width	0.16 mm

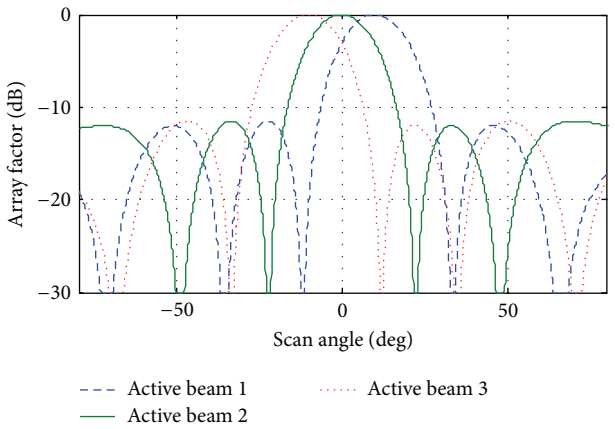

Figure 3: Array factor for three input ports excited separately.

to prevent degradation in the performance. The attenuation α_c due to the conductor loss can be determined approximately from [6]

$$\alpha_c = \frac{R_s}{(Z_0 W)} \text{ Np/mm}, \tag{4}$$

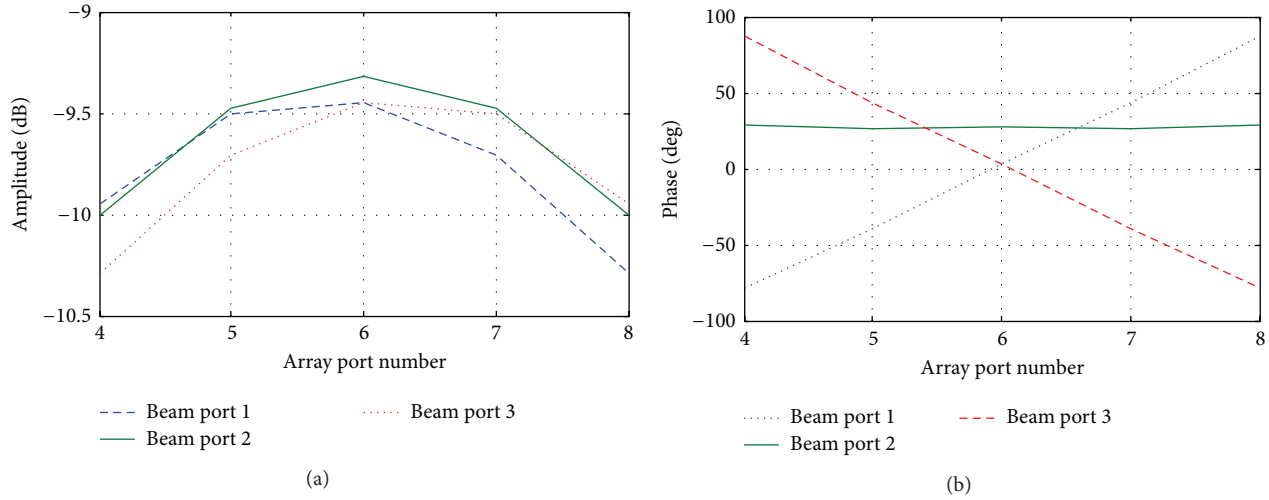

Figure 4: (a) Beam to array coupling amplitude, (b) beam to array coupling phase.

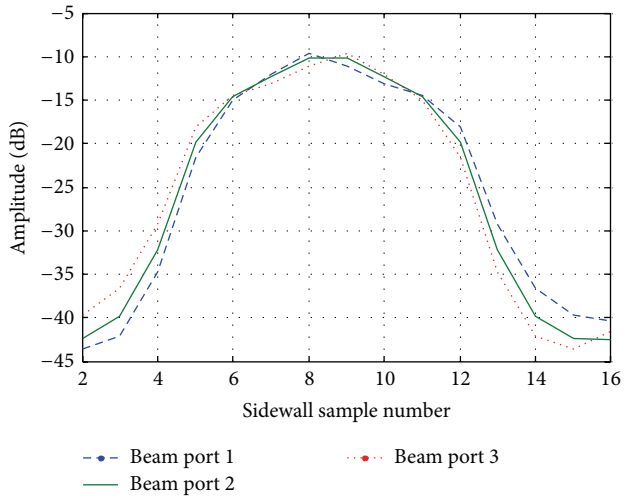

Figure 5: Beam to sidewall coupling amplitude.

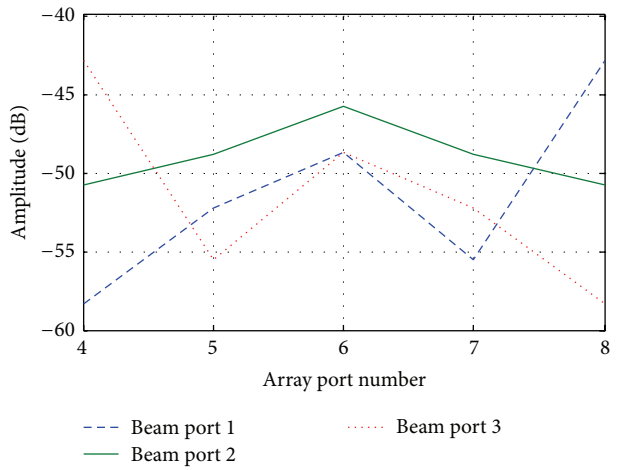

Figure 6: Beam to array spillover coupling amplitude.

where $R_s = \sqrt{\omega\mu_0/2\sigma}$ is the surface resistivity for conductor. The loss associated with the connecting transmission lines was calculated following $e^{-\alpha L}$ where $\alpha = \alpha_c + \alpha_d$ [6]. The use of high resistivity silicon to reduce substrate loss and parasitic components led to conduction between the semiconductor wafer and the metal layers in a microstrip configuration. In order to prevent current leakage to the substrate, a 100 nm thick SiO_2 layer was used between the high resistivity silicon wafer and the gold layers at the top and the bottom. A taper-matching technique with a taper width of $\lambda/2$ was used to avoid second-order mode. Through a simulation study in RLD, a total of 16 dummy ports were determined to generate low level sidelobes [8, 10, 11] while generating an optimum array factor.

Figure 2(a) shows a cross-sectional view of the designed Rotman lens and Figure 2(b) shows the top view of the lens in XFDTD 3D simulation environment. The 3D full wave simulation capabilities of XFDTD software were used to optimize the final design specifications as listed in Table 1.

3. Simulation Results

The array factors of the designed lens for three input ports excited separately are shown in Figure 3. From Figure 3, it is clear that, for each beam port excitation, the sidelobe levels are less than −12 dB. Increasing the contour curvature as well as number of the dummy ports can reduce the sidelobe levels. Low curvature lens sidewalls have much higher sidelobes. A Gaussian optimization method was used to determine the number of dummy ports to match the determined lens curvature. Phase error for individual beam port through all the array ports is calculated as low as 0.5 degrees. This amount of error is very low as compared to 14.4° [4] and 24° [12] for 77 GHz lens.

Figure 4(a) shows beam to array coupling amplitude for individual excitation of different beam ports. In worst case,

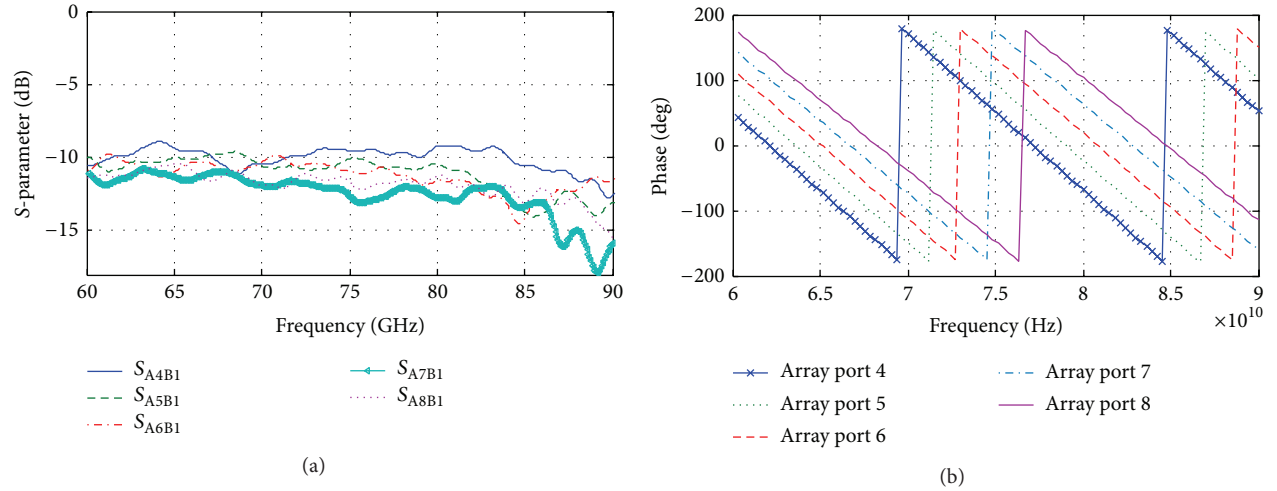

FIGURE 7: *S*-parameter for beam port number one active, (a) magnitude, (b) phase.

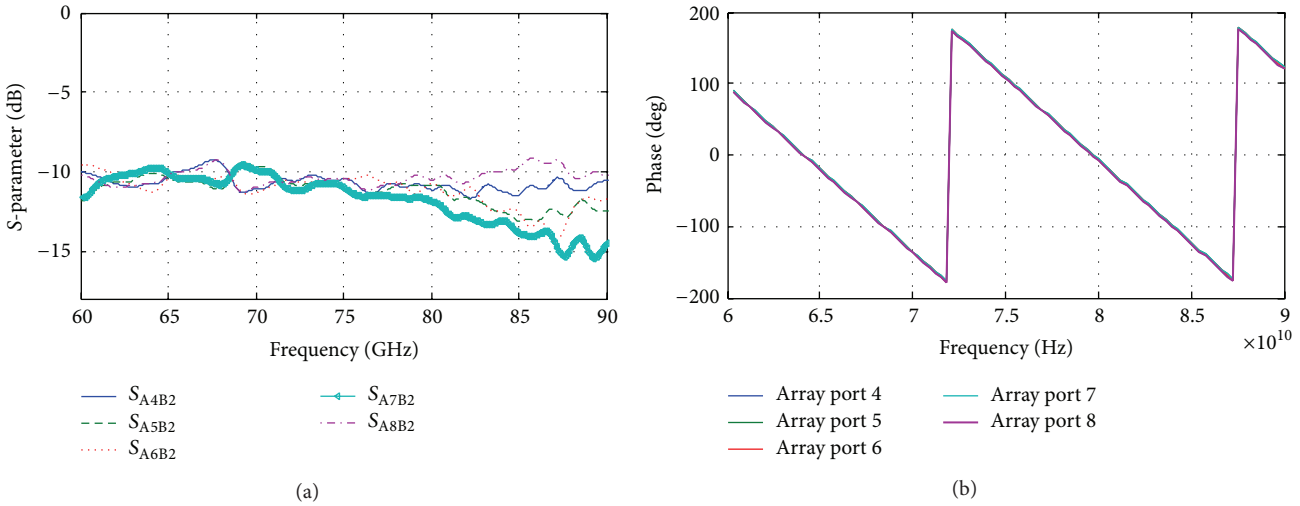

FIGURE 8: *S*-parameter for beam port number two active, (a) magnitude, (b) phase.

array port number six has the most coupling amplitude with amount of −9.45 dB for beam port number one and three and also −9.3 dB for beam port number two. Figure 4(b) shows the amount of beam to array coupling phase.

The amount of beam to sidewall coupling amplitude (coupling of energy from the beam ports into the sidewalls) among the beam ports and the 16 dummy ports (8 on each of the side walls) is shown in Figure 5. About −10 dB maximum coupling occurs for dummy ports that are close to array ports as they will absorb most of the back scattered radiation. Furthermore, beam ports to array ports spillover coupling amplitude (coupling of energy from the beam ports to array ports due to sidewall reflection) is between −58 dB to −43 dB as shown in Figure 6.

Figure 7(a) shows the *S*-parameter amplitude and Figure 7(b) shows the *S*-parameter phase for beam port 1 active for a frequency range of 60 GHz to 90. The figures show that *S*-parameter amplitudes for beam port number one along the array ports number 4, 5, 6, 7, and 8 are −11.1 dB, −11.7 dB, −11.6 dB, −12.7 dB, and −10.9 dB, respectively, and the associated phases are 3.76°, 47.44°, 87.91°, 130.40°, and 169.32°, respectively. Beam port number three has almost the same results.

Figures 8(a) and 8(b) show the *S*-parameter values, amplitude and phase, for beam port number two active. At 77 GHz all the array port phases are around 63° with a variation of 2°.

Figure 9 shows the *S*-parameters (magnitude and phase) for all the beam ports and array ports superimposed.

Figure 10 presents the return losses for individual excitation of the beam ports 1 to 3. From the figure, it is clear that the return losses associated with individual beam port excitation are in the vicinity of −10 dB.

Crosstalk is one of the consequential factors when a signal is transmitted on transmission line and produces an undesired effect in adjacent channels or transmission lines. Crosstalk is usually created by unwanted capacitive, inductive, or conductive coupling between transmission lines

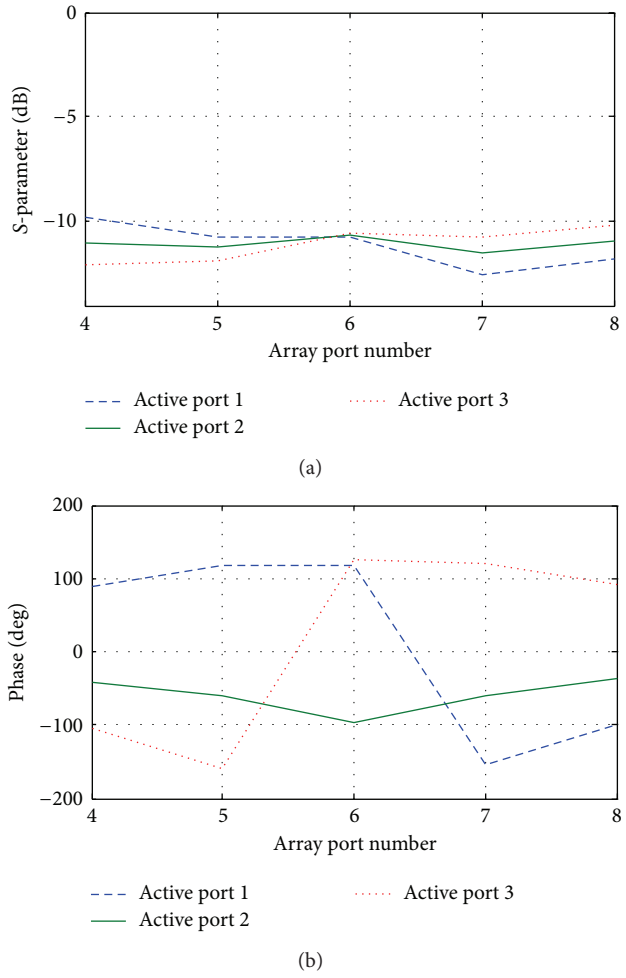

FIGURE 9: S-parameters for beam ports number one, two, and three active, (a) magnitude, (b) phase.

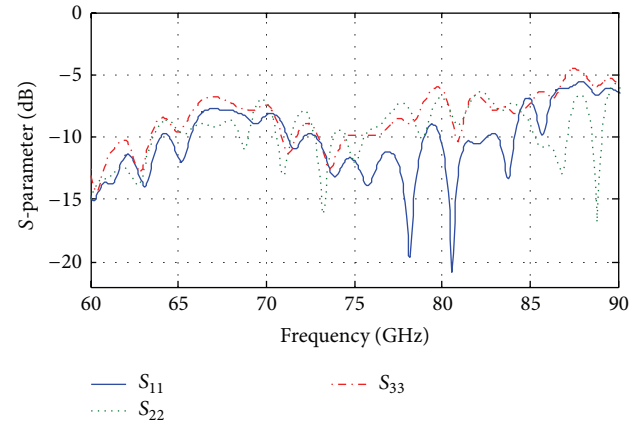

FIGURE 10: Return loss (dB) over frequency.

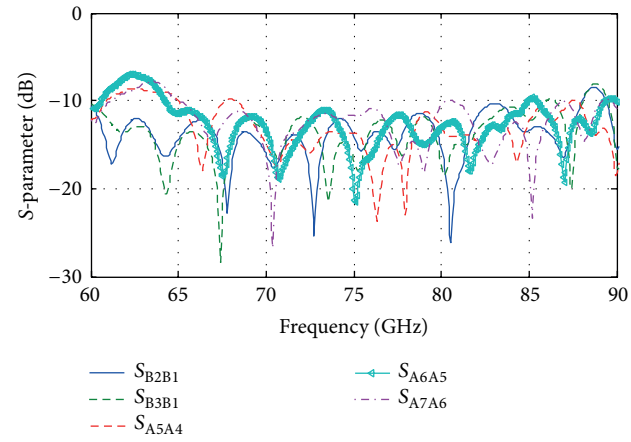

FIGURE 11: Crosstalk (dB) over frequency.

since frequency is very high and size of the wafer is shrunk. Figure 11 shows that incidence of crosstalk for all input and output lines is less than −12 dB.

Figure 12 shows that the insertion losses of beam ports 1 and 3, respectively, are 4.16 dB and for the beam port 2, the insertion loss is 3.29 dB at the center frequency of 77 GHz. It is to be noted here that, due to the maximum mesh size limitations associated with XFDTD, the 100 nm thick silicon dioxide layer was not included in XFDTD simulation to determine to insertion loss. If the 100 nm thick silicon dioxide layer could be included in simulation, the insertion loss would be much lower.

The lens efficiency can be defined as the ratio of the sum of the output power at all the array ports to the power fed at one of the beam ports [4] and can be determined from the 3D simulation results of the following transmission coefficients:

$$\text{Efficiency} = \frac{P_{\text{out}}}{P_{\text{in}}} = \sum_{n} |S_{n1}|^2 = \left(S_{41}{}^2 + S_{51}{}^2 + S_{61}{}^2 + S_{71}{}^2 + S_{81}{}^2\right). \quad (5)$$

Figure 13 shows the lens efficiency as a function of frequency for different beam port excitation. The efficiency of beam ports 1 and 3 is 34.57%, and for beam port 2 and the efficiency is 46.8% at the center frequency of 77 GHz. This proves that beam port number 2 which is in the center of the beam ports can transmit higher power to the array ports.

Figure 14 shows the E-field pattern of current propagating through the lens with beam port 2 active. The wave front will reach at all the array ports and only two closest of the dummy ports with similar amplitude levels; therefore, most of the current will be collected by the array ports. Table 2 compares the key performance parameters of the designed Rotman lens with two other similar microwave lenses.

4. Lens Fabrication Process

A 200 μm thick high resistivity (>10,000 Ω-cm) silicon wafer was RCA cleaned and a 100 nm thick layer of low temperature oxide (LTO) was grown on both sides of the wafer. A 1.5 μm thick layer of gold was deposited by e-beam evaporation onto the backside of wafer, Figure 15(a). LOR 30B lift-off resist was then spin deposited at 2000 rpm and baked at 170°C for 10 min, Figure 15(b). Shipley 1827 photoresist was then

Table 2: Comparison of key features.

Parameter	Reference [13]	Reference [14]	This paper
Frequency (GHz)	24	60	77
Material	RO3003 ($\varepsilon_r = 3$)	Silicon and SiO_2 ($\varepsilon_r = 11.7$ and 3.9)	$\varepsilon_r = 11.8$
Thickness (μm)	508	300 and 1.5	200
Length × Width (mm)	7580	19.6 × 20	19.7 × 15.6
No. of beamports	5	5	3
No. of array ports	7	7	5
Phase error (deg.)	* * *	14.4	0.5
Insertion loss (dB)	1.85	2	3.29
Return loss (dB)	Almost 10	Almost 10	Almost 10
Max. Efficiency (%)	32.30	50	46.8

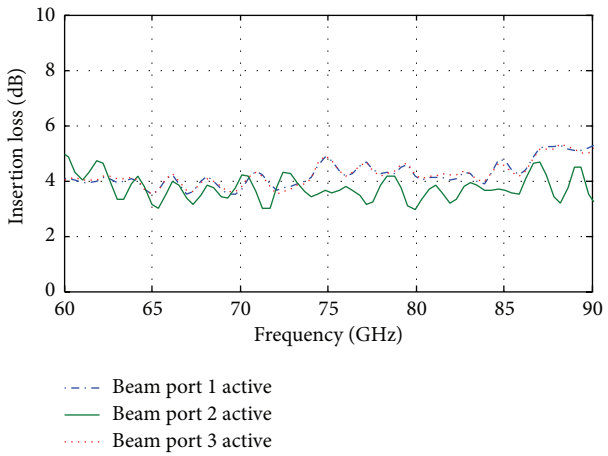

Figure 12: Insertion loss (dB) over frequency.

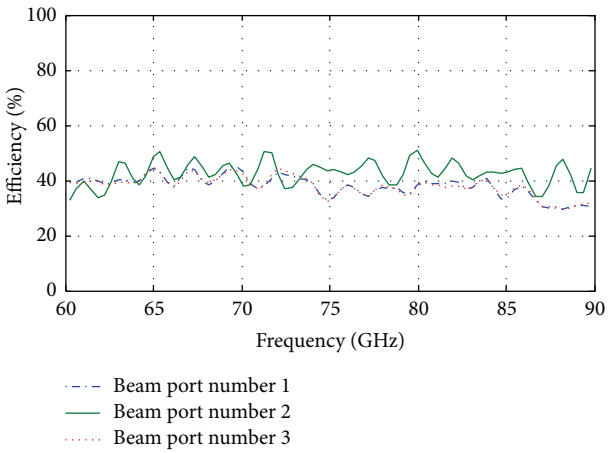

Figure 13: Power efficiency of the proposed Rotman lens for three beam ports.

spin deposited at 2500 rpm and baked 3 minutes at 113°C, Figure 15(c). The LOR and Shipley 1827 layers were then patterned with exposing the resist in the Karl Suss MA6 aligner with 540 mJ/cm^2 and developed for 3 minutes in a MF-319 dish, Figure 15(d).

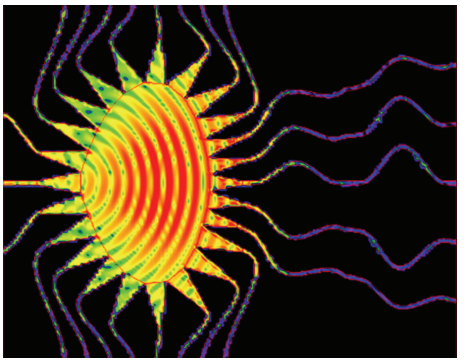

Figure 14: E-Field simulation and current propagating for beam port number two active.

Following DI water washing in the spin rinse dryer, a 1.5 micrometer thick layer of gold was deposited by e-beam evaporation, Figure 15(e), on the topside of the processed wafer. The resist was then dissolved in Remover PG during an overnight soak to complete the metal lift-off step, Figure 15(f). The wafer was then bonded to a carrier wafer with a layer of crystal bond to provide mechanical support during dicing to singulate the devices. Figure 16 shows the final fabricated lens.

5. Testing

The lens was tested in a 77 GHz radar setup. To enable testing, the lens was mounted on a special fixture along with a 77 GHz microstrip antenna array fabricated on a Duroid 5880 substrate as shown in Figure 17.

The complete test setup is shown in Figure 18. A tunable X band source was used as the RF source which was then connected to an 8 times multiplier unit to output a millimeter wave signal in the vicinity of 77 GHz. The output of the 8 times multiplier was then fed to one of the beam ports of the Rotman lens. A 77 GHz horn antenna was used to pick up the radiation from the antenna. The horn antenna was connected to an Advantest R3271A Spectrum analyzer (not in the figure) using a downconverter harmonic mixer. A screen shot of the spectrum analyzer is shown in Figure 19 where the output of the harmonic mixer was superimposed on the original

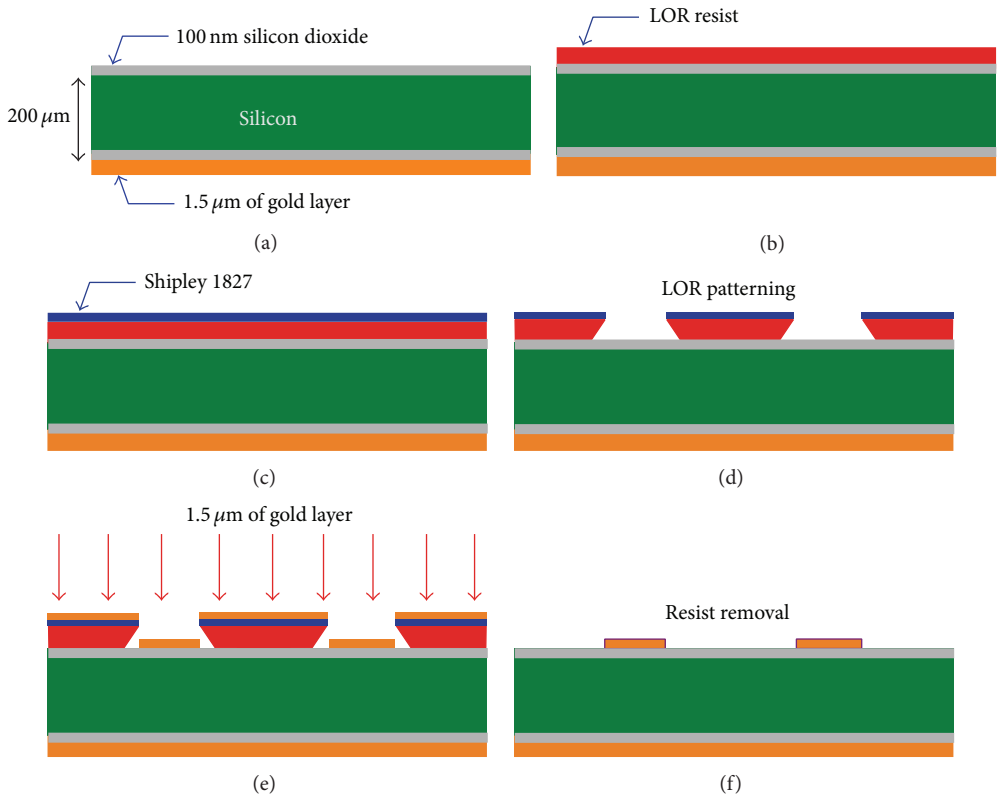

Figure 15: Fabrication steps of the proposed Rotman lens.

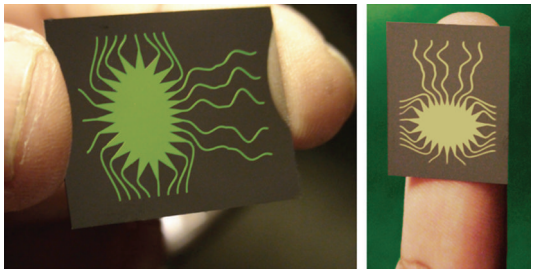

Figure 16: Fabricated Rotman lens.

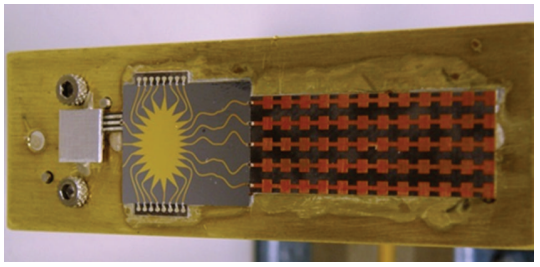

Figure 17: Fabricated Rotman lens combined with a microstrip array antenna.

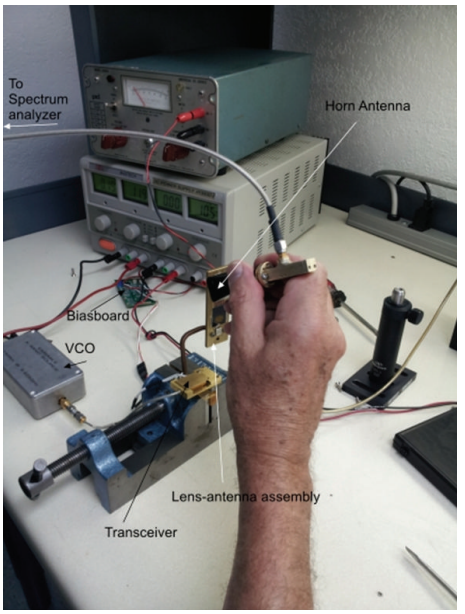

Figure 18: Complete test setup.

transmitted signal at 77 GHz. The frequency of the received signal clearly indicates that the Rotman lens is functioning properly as an integral part of the radar unit.

6. Conclusions

The design, fabrication, and testing of a high resistivity silicon wafer based 77 GHz microstrip Rotman lens have been presented. Full wave simulation of the lens was carried out

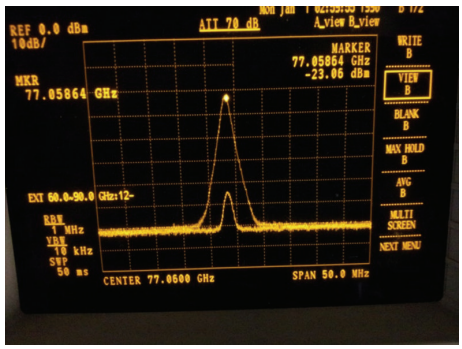

Figure 19: A screen shot of the spectrum analyzer showing both the transmitted and the received signal to verify the functionality of the Rotman lens.

using XFDTD software and the simulation results show that the lens exhibits very low phase error, compact size, and excellent RF performance. The lens has been fabricated using a lift-off process using a silicon dioxide layer between the top metal layers the silicon substrate to reduce substrate loss.

A functional test of the lens has been carried out using a 77 GHz radar setup and the test results show that the lens is working fine as designed. Further testing of the lens is in progress. The relatively less expensive microfabricated Rotman lens can be used to realize a high performance low cost MEMS based radar sensor for automotive applications by replacing expensive analog and/or digital beamformers as currently being used in commercially available automotive radar sensors. The developed Rotman lens can easily be integrated with the Radar front end circuitry and silicon based microstrip antenna array to pave the way to realize low cost high performance radar on a chip.

Conflict of Interests

The authors declare that there is no conflict of interests regarding the publication of this paper.

Acknowledgments

This research has been supported by the Natural Sciences and Engineering Research Council of Canada (NSERC)'s Discovery Grant no. RGPIN 293218, Ontario Centres of Excellence (OCE)'s Grant no. IC50659, and Auto21 NCE Canada's Grant no. F503-FSS. The authors would like to greatly acknowledge the packaging and testing support provided by Advotech Inc. of Tempe, Arizona. The authors also would like to acknowledge the supports provided by Canadian Microelectronics Corporation (CMC Microsystems).

References

[1] M. Schneider, "Automotive radar—status and trends," in *Proceedings of the German Microwave Conference (GeMiC '05)*, pp. 144–147, 2005.

[2] J. Schoebel and P. Herrero, "Planar antenna technology for mm-wave automotive radar, sensing, and communications," in *Radar Technology*, pp. 297–318, Intech, Rijeka, Croatia, 2009.

[3] R. Schneider, H.-L. Blöcher, and K. M. Strohm, "KOKON—automotive high frequency technology at 77/79 GHz," in *Proceedings of the 4th European Radar Conference*, pp. 247–250, Munich, Germany, October 2007.

[4] W. Lee, J. Kim, C. S. Cho, and Y. J. Yoon, "Beamforming lens antenna on a high resistivity silicon wafer for 60 GHz WPAN," *IEEE Transactions on Antennas and Propagation*, vol. 58, no. 3, pp. 706–713, 2010.

[5] S. Lal, R. Muscedere, and S. Chowdhury, "An FPGA-based signal processing system for a 77 GHz MEMS tri-mode automotive radar," in *Proceedings of the 22nd IEEE International Symposium on Rapid System Prototyping: Shortening the Path from Specification to Prototype (RSP '11)*, pp. 2–8, May 2011.

[6] D. M. Pozar, *Microwave Engineering*, John Wiley & Sons, New York, NY, USA, 2nd edition, 1998.

[7] W. Rotman and R. F. Turner, "Wide-angle microwave lens for line source applications," *IEEE Transactions on Antennas and Propagation*, vol. 11, no. 6, pp. 623–632, 1963.

[8] L. T. Hall, *Broadband monolithic constrained lens design [Ph.D. thesis]*, Department of Electrical Engineering, The University of Adelaide, Adelaide, Australia, 2000.

[9] D. Freundt and B. Lucas, "Long range radar sensor for high-volume driver assistance systems market," in *Proceedings of the SAE World Congress & Exhibition*, pp. 117–124, 2008.

[10] K. C. Gupta, R. Garg, I. Bahl, and P. Bhartia, *Microstrip Lines and Slotlines*, Artech House, Norwood, Mass, USA, 1996.

[11] J. Kim and F. Barnes, "Scaling and focusing of the Rotman lens," in *Proceedings of the IEEE Antennas and Propagation Society International Symposium*, pp. 773–776, Boston, Mass, USA, July 2001.

[12] I. S. Song, J. Kim, D. Y. Jung et al., "60GHz rotman lens and new compact low loss delay line using LTCC technology," in *Proceedings of the IEEE Radio and Wireless Symposium (RWS '09)*, pp. 663–666, January 2009.

[13] W. Lee, J. Kim, and Y. J. Yoon, "Compact two-layer rotman lens-fed microstrip antenna array at 24 GHz," *IEEE Transactions on Antennas and Propagation*, vol. 59, no. 2, pp. 460–466, 2011.

[14] W. Lee, J. Kim, C. S. Cho, and Y. J. Yoon, "A 60 GHz rotman lens on a silicon wafer for system-on-a-chip and system-in-package applications," in *Proceedings of the IEEE MTT-S International Microwave Symposium (IMS '09)*, pp. 1189–1192, June 2009.